NASA Technical Memorandum 103943

Measurements of Density, Temperature, and Their Fluctuations in Turbulent Supersonic Flow Using UV Laser Spectroscopy

Douglas G. Fletcher and R. L. McKenzie

October 1992

National Aeronautics and
Space Administration

NASA Technical Memorandum 103943

Measurements of Density, Temperature, and Their Fluctuations in Turbulent Supersonic Flow Using UV Laser Spectroscopy

Douglas G. Fletcher and R. L. McKenzie, Ames Research Center, Moffett Field, California

October 1992

National Aeronautics and
Space Administration

Ames Research Center
Moffett Field, California 94035-1000

Measurements of Density, Temperature, and Their Fluctuations in Turbulent, Supersonic Flow Using UV Laser Spectroscopy

D. G. Fletcher and R. L. McKenzie
Experimental Fluid Dynamics Branch
NASA Ames Research Center

ABSTRACT

Nonintrusive measurements of density, temperature, and their turbulent fluctuation levels have been obtained in the boundary layer of an unseeded, Mach 2 wind tunnel flow. The spectroscopic technique that was used to make the measurements is based on the combination of laser-induced oxygen fluorescence and Raman scattering by oxygen and nitrogen from the same laser pulse. Results from this demonstration experiment are compared with previous measurements obtained in the same facility using conventional probes and an earlier spectroscopic technique. Densities and temperatures measured with the current technique agree with the previous surveys to within 3% and 2%, respectively. The fluctuation amplitudes for both variables agree with the measurements obtained using the earlier spectroscopic technique and show evidence of an unsteady, weak shock wave that perturbs the boundary layer.

INTRODUCTION

The development of spectroscopic techniques for the investigation of turbulent, compressible flow phenomena is directed towards the simultaneous measurement of mean values and fluctuation levels for multiple gasdynamic variables [1]. One such technique has been developed for measuring density, temperature, and their turbulent fluctuations in high-speed, compressible flows using laser-induced fluorescence (LIF) of oxygen in combination with Raman scattering from oxygen and nitrogen [2,3]. The principal advantage of this approach is that flow seeding is unnecessary and measurement uncertainties due to temporal or spatial seed nonuniformity are thereby avoided. In this report we present measurements obtained with this LIF/Raman (LIF/R) technique in a turbulent, supersonic air flow. Following a description of the LIF/R technique and a discussion of the instrumentation, profiles of density, temperature, and their fluctuation amplitudes are presented for the flow boundary layer. These profiles are compared with previous results which were obtained from conventional probe and nitric-oxide (NO)-LIF measurements in the same facility [4,5]. The favorable agreement between the present and previous surveys demonstrates the ability of the LIF/R technique to accurately characterize the thermodynamic variables in unseeded, turbulent, supersonic flows.

LIF/R TECHNIQUE

Experimental investigations into the spectroscopy of both the LIF and Raman processes that guided the development of the LIF/R technique are detailed in previous publications [2,3]. The following discussion is a brief outline of the important aspects of LIF/R spectroscopy relevant to its implementation as a flow diagnostic technique.

The temperature measurement capability of the LIF/R technique is based on the use of a narrow-band, ArF-excimer laser to induce fluorescence from a single ro-vibrational transition of the oxygen Schumann-Runge system. A notable feature of this system is that the upper electronic state of the transition is perturbed by an unbound state that provides a predissociative deexcitation path for resonant oxygen molecules. For the vibrational bands accessible to the ArF laser, the predissociative depopulation rate of the upper state is at least 10^5 times faster than either collisional quenching or fluorescence decay. Since only one in 10^5 molecules fluoresce, predissociation results in a reduced signal level; but its rapidity effectively precludes collisional quenching. Another manifestation of the strong predissociation is that natural lifetime broadening dominates the transition lineshape [6] and greatly reduces the sensitivity to collisional (and Doppler) broadening and shift. With neglible influence from collisional processes, the collected fluorescence is more easily interpreted since it is linearly dependent on density through the initial state population. If the oxygen mole fraction is constant and the laser fluence not excessive, the expression for the fluorescence signal, S_F, can be written as

$$S_F = K_F \, \rho \, f_1(T) \tag{1}$$

for narrow-band excitation of a single transition, following the derivation in [2]. In the above expression, K_F is an optical and spectroscopic constant, ρ is density, and $f_1(T)$ is the temperature dependent Boltzmann population of resonant O_2 molecules in the ground state. For temperatures below 350 K, the temperature dependence of the fluorescence signal arises mainly from the thermal change of the rotational energy distribution and only the lowest vibrational level ($v'' = 0$) has significant population. The expression for $f_1(T)$ for this temperature range is

$$f_1(T) = (2K'' + 1) \, \frac{2\theta_r}{T} \, exp[-K''(K'' + 1)(\theta_r/T)] \tag{2}$$

where K'' is the ground state rotational quantum number, θ_r is the characteristic rotational temperature (2.1 K), and T is temperature.

Depending on the anticipated range of temperatures, the laser is tuned to resonance with a rotational transition that has been selected for suitable temperature sensitivity and signal level. Figure 1 illustrates the fluorescence signal temperature dependence at constant density given by equation (2) for two different rotational transitions of the ($4 \leftarrow 0$) vibrational band. Signals for each transition are normalized by their respective values at 300 K. The transition with the higher rotational quantum number, $R19$, has greater temperature sensitivity over the whole range as

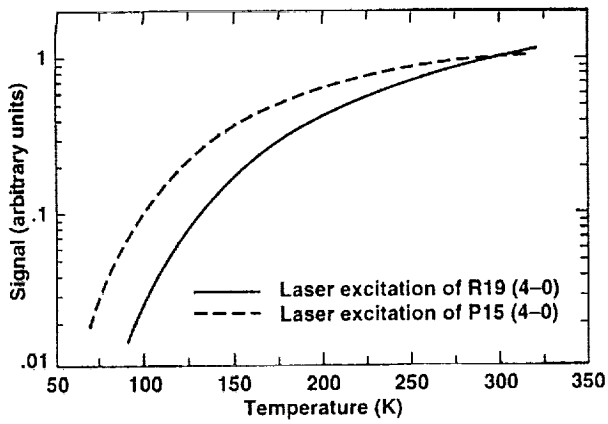

Figure 1. Variation of LIF signals with temperature for two different rotational transitions.

shown by the steeper slope of the solid line. Signal strength for the $R19$ transition is sufficient for temperature measurements above 100 K. However, the signal is very weak below 100 K due to relatively low population, and the greater population of the $P15$ transition makes it a better choice for measurements at lower temperatures.

There have been several demonstrations of temperature measurement using LIF of oxygen at constant pressure [2,3,7-11]. Most of these experiments were directed toward high-temperature applications, such as flame diagnostics, where the higher vibrational levels of the ground electronic state are significantly populated. Another technique for measuring temperatures at varying density or pressure relies on a two-transition approach [12]. However, if density is measured independently during the same laser pulse, the density dependence of the LIF signal can be accounted for and temperature can then be derived from the fluorescence variation of a single transition [13].

Spontaneous Raman scattering by oxygen and nitrogen molecules provides a convenient, independent measurement of density that is also used to account for the density dependence of the fluorescence. Any temperature sensitivity of the Raman signals is removed by spectrally integrating the total Q-branch scattering. Since the spontaneous Raman cross-section varies as frequency to the fourth power, Raman scattering is more efficient at ultraviolet wavelengths. In addition, the oxygen Raman cross-section is considerably enhanced by near-resonant contributions within the Schumann-Runge band that increase the scattered light level by a factor of 22 over the expected level near 193 nm [14].

The Raman signal, S_R, for constant air composition can be simply written as

$$S_R = K_R \, \rho \tag{3}$$

where K_R is an optical and spectroscopic constant. Density measurements are obtained directly from equation (3) and temperature measurements are derived from the variation of the fluorescence signal (equ. (1)) divided by the Raman signal (equ. (3)),

$$S_F/S_R = (K_F/K_R) \, f_1(T) \tag{4}$$

Equations (3) and (4) are the basic relations used in this work. In practice however, the ArF laser induces fluorescence from additional transitions due to spectral overlap with both narrow-band and unlocked, broad-band radiation. (Not all of the amplified laser emission is narrow-band when the laser is operated in the multipass amplifier configuration.) For this reason a numerical model of the O_2-LIF process [2] is used to evaluate equation (4).

EXPERIMENTAL CONSIDERATIONS FOR THE LIF/R TECHNIQUE

The optical configuration for implementation of the LIF/R technique is shown in Fig. 2. Pulses from a tunable, ArF-excimer laser are delivered to the wind tunnel at a rate of 10 Hz and are focussed to a 0.5 mm by 1 mm spot at the measurement location. Portions of the beam are split off before and after the wind tunnel and directed to photodiodes to account for laser-pulse energy fluctuations and varying attenuation. The LIF and Raman signals emanating from the laser probe volume are collected with a two-lens telescope (magnification = 3.3) and dispersed by a 0.32 m spectrometer fitted with a 1200 $line/mm$ holographic grating. An entrance slit width of 0.5 mm limits the observed length of the probe volume to 0.15 mm for the pointwise measurements. The dispersed spectrum is recorded by an optical multichannel analyzer (OMA) and stored in a personal computer along with the photodiode signals from the same laser pulse. Both the OMA and the gated integrator are controlled by a single personal computer using PC-DOS and multitasking software. Exposure of the OMA to the 15 $nsec$ laser pulse is controlled through gating of the intensifier on the photodiode array. As shown on the figure, the OMA is triggered at twice the laser repetition rate to clear the array of accumulated signal from previous laser pulses. These signal remnants are caused by slow radiative decay of the intensifier phosphor (P-20 for this OMA) and they generate a persistant image that can compromise single-pulse spectral measurements [15].

An investigation of the magnitude of the image persistance effect for the OMA used in this work and its reduction for different array cleaning schemes is summarized in Fig. 3. The figure shows the image persistence, which is defined as the percentage of the original image read off of the array following a trigger pulse, as a function of time. Up to time $t = 0$, the OMA has been exposed to light signals induced by laser pulses at a rate of 10 Hz (0.1 sec between pulses). At $t = 0$, the laser light is blocked, but the OMA array is still read at each trigger pulse. Signals read from the array after the light is blocked represent the sum of decaying signal remnants from previous exposures that remain as an image on the long-lived intensifier phosphor. The circular symbols represent the basic image persistance level of the OMA for an array temperature of 20°C with no cleaning between laser pulses. Signals are only read from the OMA each time the laser fires. At the time of the first laser pulse following the block, 20% of the initial signal remains. After five pulses, the remaining signal has decayed to about 3% of the original level. The solid line through the circles is a power law fit to the data ($\propto t^{-n}$). If a single cleaning pulse is supplied to the OMA between laser shots, the image persistance is substantially reduced, as shown by the square symbol distribution. With the additional read between laser shots, 4% of the original signal level remains on the array at the time of the second laser pulse and about 1% is left

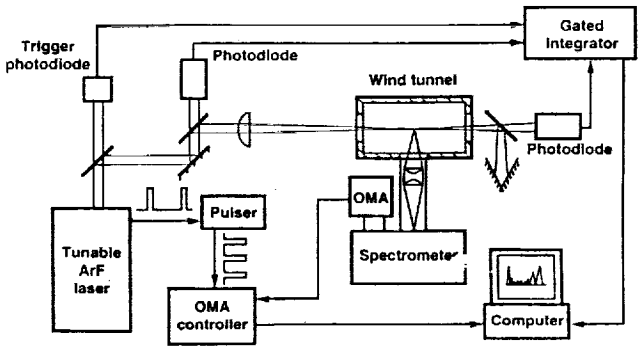

Figure 2. Experimental arrangement for the application of the LIF/R technique to the investigation of a turbulent, supersonic boundary layer flow.

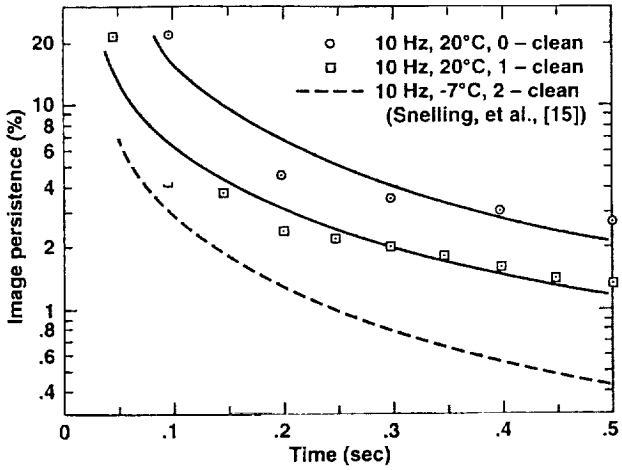

Figure 3. The magnitude of the image persistence effect for the OMA used in the LIF/R demonstration experiment and it's reduction for different cleaning pulse schemes. The dashed line represents data measured by Snelling et al. [15] for the same instrument with two cleaning pulses.

after five pulses. The dashed curve represents the image persistence measured by Snelling et al. [15] for the same OMA using a variably-timed triggering scheme with two cleaning pulses. Their array was operated at a lower temperature, $-7°C$ which weakly increases the persistence level. For two cleaning pulses between laser shots, there is a further reduction in the image persistence to less than 3% after the first laser shot and to less than 0.5% after five laser shots. However, due to the ease of adding the single cleaning pulse and operating the array at $20°C$ to minimize the image persistence, the single cleaning pulse OMA-triggering method was adopted for these experiments.

Despite the fact that not all of the persistant image is removed by the cleaning pulse before the subsequent laser shot, the remnant is only 4% of the mean signal level. If the number of shots acquired for each measurement is constant, then the additional signal contributions from image persistence are constant fractions of the average signals. This constant contribution cancels when the measured signal is calibrated against a signal level from a known reference condition, as illustrated by the Raman-signal based density measurement,

$$\rho = (S_R/S_{Rcal})\rho_{cal} \tag{5}$$

The mean property values are, therefore, unaffected by the phosphor lag. Temperature fluctuation measurements are also unaffected by image persistence because temperatures are derived from the LIF signals divided by the Raman signals for each laser pulse (see equ. (4)). Normalizing the LIF signals in this manner involves dividing the signals from photodiodes on one side of the array by photodiode signals on the other side of the array. This removes the persistent signal contribution directly for each fluorescence record since all photodiodes of the array are affected equally by the accumulaton of previous signal remnants. However, the Raman signals are not corrected in the same manner and the image persistence adds an estimated uncertainty to the density fluctuation amplitude measurement of about 5% for random signal variations due to turbulence. Although an OMA is not specifically required for the application of the LIF/R technique, the instrument is useful for initial flow field investigations because the spectral record includes the wavelength distribution of the signals as well as their magnitude. This additional information is helpful in determining the level and source of undesirable emission from either flow contaminants or competing spectroscopic processes (see p. 4878 of [2], for example).

TURBULENT, SUPERSONIC, AIR FLOW FACILITY

The wind tunnel used for the demonstration measurements is a Mach 2, blow-down facility that has a rectangular cross section for providing two-dimensional flow. A schematic representation of the tunnel is shown in Fig. 4. Clean, dry air at high pressure and room temperature is expanded through a Laval nozzle into a long, slightly-divergent flow channel which was designed to provide fully turbulent flow and to accomodate boundary layer growth on the top and bottom walls. At the measurement location, 0.76 m downstream of the throat, the test section is 32.5 mm high by 63 mm wide, the free stream Mach number is 2.06, and the boundary layer is 12.1 mm thick. Laser beam access is provided through two ultraviolet-grade fused silica windows and light signals are collected through an identical window in the top wall. For the current setup, the long dimension of the rectangular laser spot is oriented perpendicular to the bottom wall of the tunnel and this limits the spatial resolution of the present boundary layer survey to 1 mm. A pressure tap is located on the bottom wall at the measurement location directly opposite the collection window and is used to record the static pressure during the run and calibration measurements. Since the blow-down is a constant-volume expansion process, both the stagnation pressure and stagnation temperature decrease during the run. A thermocouple upstream of the Laval nozzle and a pressure tap in the storage vessel are used to monitor the changing reservoir conditions. The time-averaged stagnation conditions and important boundary layer properties for the flow facility are summarized in Table 1. Flow centerline pressure and temperature at Mach 2.06 are nominally 32 kPa and 157 K for the given stagnation conditions. The total run duration is 15 sec and the useful steady-flow measurement time is about 13 sec. For a laser repetition rate of 10 Hz, at least 90 signal records can be acquired during a typical wind tunnel run. Previous surveys of the boundary layer by pitot

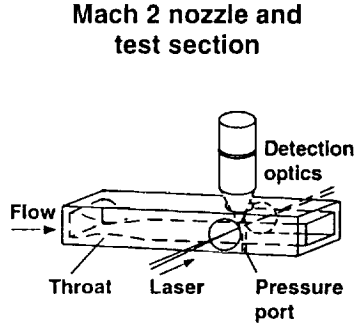

Figure 4. Mach 2 wind tunnel used for the LIF/R demonstration experiment. The flow property survey was done in the bottom-wall boundary layer.

Table 1. Time-averaged properties and characteristics of the turbulent, Mach 2 flow boundary layer.

M_∞	2.06
U_∞	517 m/sec
δ	12.1 mm
Re_x	2.7×10^7
Re_δ	4.4×10^5
T_{stag}	290 K
P_{stag}	270 kPa

probe, hot wire anemometer, thermocouple probe, and an NO-LIF spectroscopic technique have characterized the mean property and turbulent fluctuation variations in the flow [4,5]. These surveys provide a useful benchmark for assessing the performance of the present LIF/R optical technique. The only difference in the operation of the wind tunnel for the current experiments is that air is used as the flow gas whereas the previous measurements were undertaken in nitrogen.

LIF/R MEASUREMENT RESULTS

The implementation of the LIF/R technique in the wind tunnel requires that spectra collected during the tunnel run be compared with an emission spectrum acquired at known density and temperature for calibration of the signal levels. This aspect of the technique is illustrated in Fig. 5, which compares an averaged spectrum from the wind tunnel boundary layer with a calibration spectrum acquired at the same location in still air after the tunnel run. The laser is resonant with the $R19$ $(4 \leftarrow 0)$ transition and each spectrum represents the average of 95 spectra that are normalized by laser-pulse energy measurements. The mean flow and mean calibration conditions for the spectra are given in the figure legend. Signal levels for the emission features are plotted versus wavelength. The O_2 and N_2 Raman transitions are located on the left and the O_2-LIF emission features on the right are identified by the difference in their final and inital ground state vibrational quantum numbers. The fluorescence transitions used for the temperature measurements are $\Delta v'' = 4$, 5, 6, and 7. A lower density during the wind tunnel run is directly measured by the reduction in Raman signal levels. The lower level of the mean LIF signal for the wind tunnel run is due to both the decreased density and a lower temperature. The Raman and LIF signals for each laser pulse are obtained by integrating the selected features over their respective wavelengths for each individual spectrum. Density and temperature values for each pulse during the wind tunnel run are then derived by comparing the signal levels with the mean calibration values at the known reference conditions. An additional result of the calibration spectrum acquisition for quiescent air is the simultaneous determination of the instrumental noise level in the absence of turbulent fluctuations. Single-pulse departures from the mean of the measured property values during the wind tunnel run are due to a combination of turbulent fluctuations and instrumental noise, and each contribution is statistically independent of the other. Therefore, the square of the calibration deviations can be subtracted from the square of the tunnel run deviations to remove the instrumental noise from the total fluctuation level and determine the turbulent fluctuation amplitude. Typical values of the instrumental noise level for these experiments were 4% for density and 3% for temperature.

Mean flow property measurements from the LIF/R boundary layer survey are compared in Fig. 6 with results from the previous experiments [4]. All measured flow properties are normalized by their respective values in the free stream at the flow centerline and the measurement locations are shown as the distance from the bottom wall normalized by the boundary layer thickness, δ. The upper dashed line is the temperature distribution that was derived from pitot-probe and thermocouple-probe surveys. The flow temperature shows a monotonic decrease from the adiabatic wall value to the free stream value. In the absence of an external pressure gradient, the probe-measured static pressure is constant through the boundary layer, as shown by the solid line. The density variation was obtained from the temperature and pressure distributions using the ideal gas equation of state and is shown by the lower dashed line. (Although previous measurements of the mean flow properties were obtained with the NO-LIF technique [4], the results are not shown because they did not differ from the probe-measured distributions.) Open symbols represent measurements of mean flow density and temperature using the LIF/R technique. The mean values obtained thus far agree with the previous measurements to within 3% for density and 2% for temperature. Through the ideal gas equation of state, the LIF/R-measured densities and temperatures are used to derive the static pressure distribution, which is denoted on the figure by the solid squares. As expected, static pressure is constant to within 2% through the boundary layer.

The uncertainty levels for these LIF/R measurements are relatively high due to a strong instrumental noise contribution from the image intensifier that is used to gate the OMA. This intensifier noise was larger than the photon-statistical noise contribution for the measured signal levels. Consequently, the total instrumental noise was effectively constant for a large range of signals and the uncertainty for both variables can be calculated using the following relations,

$$\left(\frac{\Delta\rho}{\rho}\right)_r = \left[\left(\frac{\Delta\rho}{\rho}\right)_c^2 + 2\left(\frac{\Delta S_R}{S_R}\right)_c^2\right]^{1/2} \qquad (6)$$

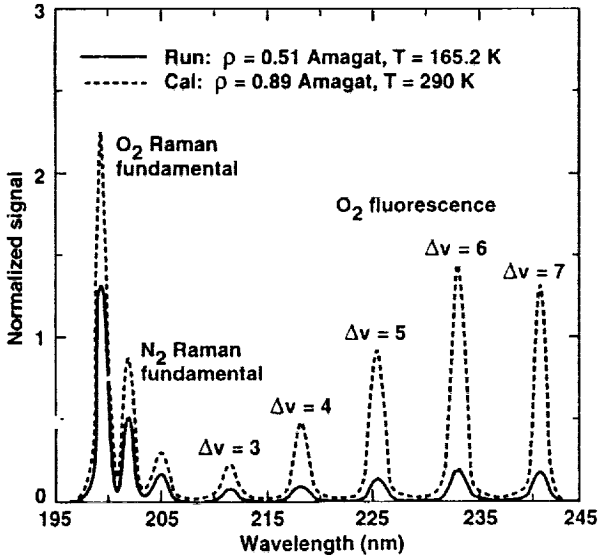

Figure 5. A comparison of the emission spectrum recorded in the turbulent Mach 2 boundary layer with the emission spectrum at the same location in still air after the wind tunnel run. The spectra were obtained at $Y/\delta = 0.68$ above the bottom wall.

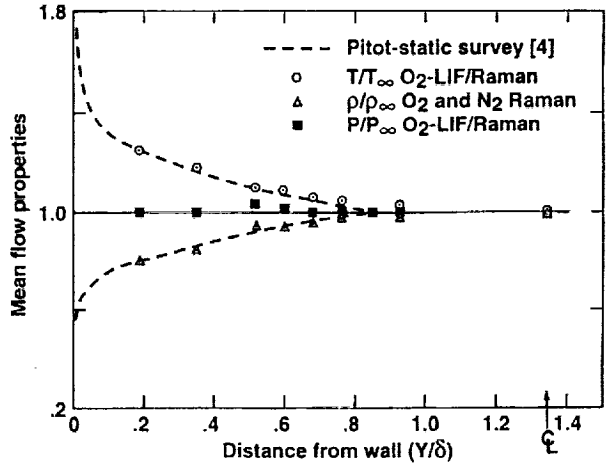

Figure 6. LIF/R measurements of mean density and mean temperature in the turbulent, Mach 2 boundary layer are compared with results from previous surveys. The mean values at each location are normalized by their respective free stream values.

$$\left(\frac{\Delta T}{T}\right)_r = \left[\left(\left(\frac{B}{T_c}-1\right)\frac{\Delta T}{T}\right)_c^2 + 2\left(\frac{\Delta S_F}{S_F}\right)_c^2 + 2\left(\frac{\Delta S_R}{S_R}\right)_c^2\right]^{1/2} \Big/ \left(\frac{B}{T_r}-1\right) \qquad (7)$$

In the above expressions, $\Delta\rho/\rho$ is the density uncertainty and $\Delta T/T$ is the temperature uncertainty. $\Delta S_F/S_F$ and $\Delta S_R/S_R$ are the LIF and Raman signal uncertainties and both are given by the measured instrumental noise levels discussed earlier (0.03 and 0.04, respectively). The subscript r refers to the value measured during the tunnel run and the subscript c refers to the calibration value. The constant in the temperature sensitivity factor is the rotational energy level, $B = K''(K''+1)\theta_R$. For the $R19$ transition, the ground state rotational quantum number, $K'' = 19$. The uncertainties in the reference values of density and temperature were about 1% . Using these values and the above relations, the uncertainties for the LIF/R boundary layer survey were 5.5% for density and 2.5% for temperature. Agreement between the LIF/R measurements and previous results is within the uncertainty for both variables.

Comparisons of the fluctuation amplitude distributions measured by the LIF/R technique with those from the previous measurements are shown in Fig. 7a for temperature and in Fig. 7b for density. The root-mean-square (RMS) fluctuation amplitude is the average deviation level divided by the local mean property value. Both variables are again plotted as a function of the nondimensional distance from the bottom wall. The solid line in each figure is a cubic spline interpolation of the hot-wire anemometer measurements of Logan et al. [5].

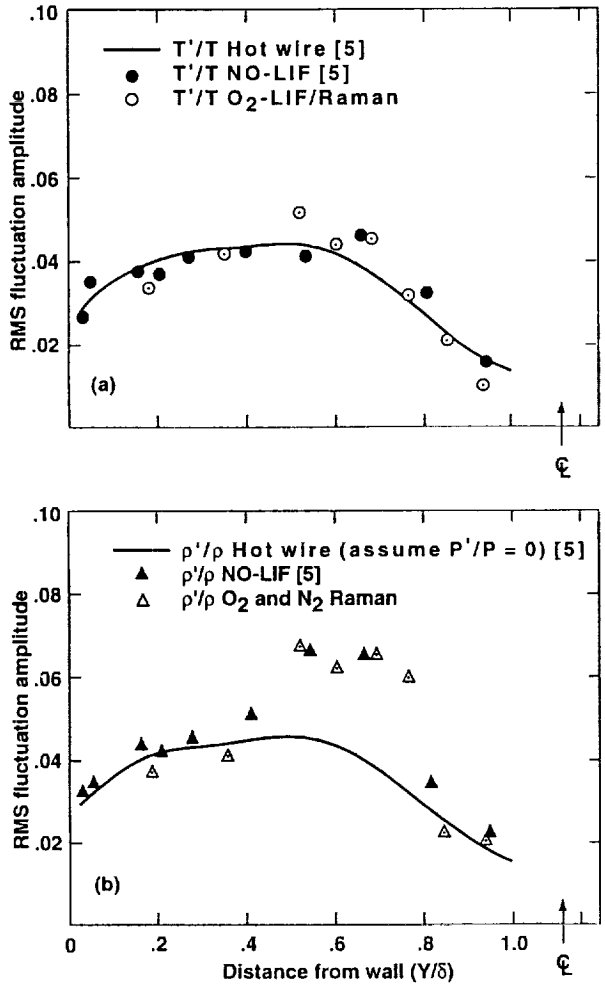

Figure 7(a) A comparison of the RMS temperature fluctuations measured with the LIF/R technique in the turbulent Mach 2 boundary layer with previous measurements from hot-wire and NO-LIF surveys, (b) a comparison of the RMS density fluctuations measured with the LIF/R technique in the turbulent Mach 2 boundary layer with previous measurements from hot-wire and NO-LIF surveys.

In Fig. 7a, the RMS temperature fluctuation amplitudes measured with the LIF/R technique are denoted by the open circles and the NO-LIF values from [4,5] are represented by the solid circles. Each of the independently measured temperature fluctuation distributions shows the same basic trend throughout the boundary layer. The maximum temperature fluctuation amplitude of about 4.5% occurs near $Y/\delta = 0.6$, and in that region the optically-measured amplitudes are slightly greater than the hot-wire measurements.

For the RMS density fluctuations in Fig. 7b, the LIF/R measurements are the open triangles and the NO-LIF results from [4,5] are shown by the solid triangles. In the figure, there is some disagreement between the measured distributions that is quite pronounced near $Y/\delta = 0.6$. Both of the optically-measured profiles show a substantially higher value for density fluctuations in this region than indicated by the hot-wire measurements. In the previous studies, this increase in density fluctuation level was attributed to an unsteady, weak shock wave that moves intermittently through the measurement location. Histograms of more than 300 single-pulse density measurements from the NO-LIF technique [16] show a bimodal distribution in this region, which supports the hypothesis that an unsteady wave is present. While the preliminary LIF/R density record also inicates a bimodal distribution near $Y/\delta = 0.6$, there are not yet a sufficient number of measurements to be conclusive. As described in [5], the relative change in flow properties caused by the unsteady wave movement can be evaluated using the weak shock relations [17].

$$\frac{\Delta\rho}{\rho} = \frac{1}{\gamma-1}\frac{\Delta T}{T}, \qquad \frac{\Delta P}{P} = \gamma\frac{\Delta\rho}{\rho} \qquad (8a, b)$$

where P is the static pressure and γ is the ratio of specific heats. The symbol Δ here represents the change in properties from the upstream side of the weak shock to the downstream side. For a diatomic gas with $\gamma = 7/5$, the density change across a weak shock wave is 2.5 times greater than the change in temperature. Therefore, the effect of the weak wave movement is more readily apparent in the density fluctuation distribution than in the temperature fluctuations. Pressure variation for the same weak shock process is even stronger (1.4 times greater than the density variation for $\gamma = 7/5$). However, to obtain density fluctuation amplitudes from hot-wire measurements, pressure fluctuations are assumed to be negligible. This assumption is inappropriate for this flow and the weak-shock driven increase in the density fluctuation level to 6.5% near $Y/\delta = 0.6$ could not be measured with the hot-wire anemometer.

CONCLUSIONS

The measurements of density, temperature, and their fluctuations in the Mach 2 boundary layer represent the first application of the LIF/R technique to the investigation of an unseeded, turbulent, supersonic flow. For each of the measured variables, the agreement between the present and previous results demonstrates the ability of the LIF/R technique to accurately characterize the mean and fluctuating components in a typical wind tunnel.

With a single cleaning pulse and an array temperature of $20°C$, the OMA image persistence has a negligible affect on all flow property measurements. The instrumental noise level for the present experiment is dominated by a strong contribution from the OMA intensifier that is larger than the photon-statistical noise contribution. This noise level is relatively high and it limits the uncertainty of the measurements to 5.5% for density and 2.5%

for temperature. The LIF/R technique does not require an OMA and efforts are underway to repeat the boundary layer survey with reflective filters and photomultiplier tubes in place of the OMA and spectrometer. The results of the repeated surveys will guide further development of instrumentation for applications to hypersonic flows.

REFERENCES

1. A. C. Eckbreth, "Laser Diagnostics for Combustion Temperature and Species," Abacus Press, Cambridge, 1988.
2. G. Laufer, R. L. McKenzie, and D. G. Fletcher, *A Method for Measuring Temperatures and Densities in Hypersonic Wind Tunnel Air Flows Using Laser-Induced O_2 Fluorescence*, Applied Optics **29** (1990), 4873-4883.
3. D. G. Fletcher and R. L. McKenzie, *Simultaneous Measurements of Temperature and Density in Air Flows Using UV Laser Spectroscopy*, LIA Conf. Proc. **72** (1991), 11-19.
4. K. P. Gross, R. L. McKenzie, and P. Logan, *Simultaneous Measurements of Temperature, Density, and Pressure in Supersonic Turbulence Using Laser-Induced Fluorescence*, Experiments in Fluids **5** (1987), 372-380.
5. P. Logan, R. L. McKenzie, and D. Bershader, *Hot-Wire Accuracy in Supersonic Turbulence from Comparisons with Laser-Induced Fluorescence* AIAA Journal **26** (1988), 316-322.
6. B. R. Lewis, L. Berzins, J. H. Carver, and S. T. Gibson, *Rotational Variation of Predissociation Linewidth in the Schumann-Runge Bands of $^{16}O_2$*, JQSRT **36** (1986), 187-207.
7. M. P. Lee, P. H. Paul, and R. K. Hanson, *Quantitative Imaging of Temperature Fields in Air Using Planar Laser-Induced Fluorescence of O_2*, Optics Letters **12** (1987), 75-77.
8. R. A. Copeland, P. C. Cosby, D. R. Crosley, J. B. Jeffries, and T. G. Slanger, *Vibrationally Excited O_2 in Flames: Measurements on $v'' = 9 - 11$ by Laser-Induced Fluorescence*, J. Chem. Phys. **86** (1987), 2500-2504.
9. P. Andresen, A. Bath, W. Gröger, H. W. Lülf, G. Meijer, and J. J. ter Meulen, *Laser-Induced Fluorescence with Tunable Excimer Lasers as a Possible Method for Instantaneous Temeperature Field Measurements at High Pressures: Checks With an Atmospheric Flame*, Applied Optics **27** (1988), 365-378.
10. C. Lalo, J. Masanet, J. Deson, R. Ben-Aim, and J. Rostas, *Temperature Measurement in a CO_2 Laser Beam by Laser-Induced Fluorescence of O_2*, Applied Spectroscopy **44** (1990), 442-447.
11. G. S. Kim, L. M. Hitchcock, E. W. Rothe, and G. P. Peck, *Identification and Imaging of Hot O_2 ($v'' = 2$, 3, or 4) in Hydrogen Flames Using 193 nm- and 210 nm-Range Light*, Applied Phys. B **53** (1991), 180-186.
12. M. S. Smith, L. L. Price, and W. D. Williams, *Laser-Induced Fluorescence Diagnostics Using a Two-Line Excitation Method*, AIAA Paper 92-0512 (1992).
13. R. B. Miles, J. J. Connors, P. J. Howard, E. C. Markovitz, and G. J. Roth, *Proposed Single-Pulse Two-Dimensional Temperature and Density Measurements of Oxygen and Air*, Optics Letters **13** (1988), 195-197.
14. W. K. Bischel and G. Black, *Wavelength Dependence of Raman Scattering Cross Sections from 200-600 nm*, AIP Conf. Proc. Vol. 100, 181-187, 1983.
15. D. R. Snelling, G. J. Smallwood, and R. A. Sawchuk, *Nonlinearity and Image Persistence of P-20 Phosphor-Bases Intensified Photodiode Array Detectors Used in CARS Spectroscopy*, Applied Optics **28** (1989), 3226-3232.
16. P. Logan, *Studies of Supersonic Turbulence and Hot-Wire Response Using Laser-Induced Fluorescence*, Ph.D. Dissertation, Stanford Univ., Stanford, CA (1987).
17. H. W. Liepmann and A. Roshko, "Elements of Gasdynamics," Wiley, New York, 1957, p. 65.

REPORT DOCUMENTATION PAGE

Form Approved
OMB No. 0704-0188

1. AGENCY USE ONLY *(Leave blank)*	2. REPORT DATE	3. REPORT TYPE AND DATES COVERED
	October 1992	Technical Memorandum

4. TITLE AND SUBTITLE

Measurements of Density, Temperature, and Their Fluctuations in Turbulent Supersonic Flow Using UV Laser Spectroscopy

5. FUNDING NUMBERS

505-59

6. AUTHOR(S)

Douglas G. Fletcher and R. L. McKenzie

7. PERFORMING ORGANIZATION NAME(S) AND ADDRESS(ES)

Ames Research Center
Moffett Field, CA 94035-1000

8. PERFORMING ORGANIZATION REPORT NUMBER

A-92120

9. SPONSORING/MONITORING AGENCY NAME(S) AND ADDRESS(ES)

National Aeronautics and Space Administration
Washington, DC 20546-0001

10. SPONSORING/MONITORING AGENCY REPORT NUMBER

NASA TM-103943

11. SUPPLEMENTARY NOTES

Point of Contact: Douglas G. Fletcher, Ames Research Center, MS 229-1, Moffett Field, CA 94035-1000; (415) 604-6229
Presented at the Sixth International Symposium on Applications of Laser Techniques to Fluid Mechanics, Lisbon, Portugal, July 20-23, 1992.

12a. DISTRIBUTION/AVAILABILITY STATEMENT

Unclassified — Unlimited
Subject Category 35

12b. DISTRIBUTION CODE

13. ABSTRACT *(Maximum 200 words)*

Nonintrusive measurements of density, temperature, and their turbulent fluctuation levels have been obtained in the boundary layer of an unseeded, Mach 2 wind tunnel flow. The spectroscopic technique that was used to make the measurements is based on the combination of laser-induced oxygen fluorescence and Raman scattering by oxygen and nitrogen from the same laser pulse. Results from this demonstration experiment are compared with previous measurements obtained in the same facility using conventional probes and an earlier spectroscopic technique. Densities and temperatures measured with the current technique agree with the previous surveys to within 3% and 2%, respectively. The fluctuation amplitudes for both variables agree with the measurements obtained using the earlier spectroscopic technique and show evidence of an unsteady, weak shock wave that perturbs the boundary layer.

14. SUBJECT TERMS

Density and temperature measurements, Laser-induced fluorescence, Oxygen fluorescence, Raman scattering, Turbulent boundary-layer measurements, Supersonic flow, and Nonintrusive flow diagnostic

15. NUMBER OF PAGES

9

16. PRICE CODE

A02

17. SECURITY CLASSIFICATION OF REPORT	18. SECURITY CLASSIFICATION OF THIS PAGE	19. SECURITY CLASSIFICATION OF ABSTRACT	20. LIMITATION OF ABSTRACT
Unclassified	Unclassified		